Generated using the official AMS LaTeX template v6.1 two-column layout. This work has been submitted for publication. Copyright in this work may be transferred without further notice, and this version may no longer be accessible.

# Topographically-generated near-internal waves as a response to winds over the ocean surface

Ashley J. Barnes,[a] Callum J. Shakespeare[a], Andrew McC. Hogg,[a] and Navid C. Constantinou,[a]

[a] *Research School of Earth Sciences & ARC Centre of Excellence for Climate Extremes, Australian National University, Canberra, Australia*

ABSTRACT: Internal waves propagate on the ocean stratification and carry energy and momentum through the ocean interior. The two most significant sources of these waves in the ocean are surface winds and oscillatory tidal flow across topography. We propose a hybrid of these two mechanisms, in which wind induced oscillations of sea surface and isopycnal heights are rapidly communicated to the seafloor via hydrostatic pressure. In the presence of topography, the resulting oscillatory bottom velocity may then generate internal waves in a similar manner to the barotropic tide. We investigate this mechanism in an idealised numerical isopycnal model of a storm passing over a mid ocean ridge, and perform several perturbation experiments in which ocean and wind properties are varied. Bottom-generated internal waves are identified propagating away from the ridge in the wake of the storm. Estimates of the total wave energy suggest that in the right circumstances these waves could be a significant source of internal wave energy, with a local wind work to wave energy conversion rate of up to 50% of the corresponding conversion to surface generated near-inertial waves in our domain. Our results suggest a need for further investigation in less idealised scenarios to more precisely quantity this novel mechanism of deep ocean wave generation, and how it may affect abyssal mixing.

SIGNIFICANCE STATEMENT: The ocean is stratified: denser waters are in the ocean abyss and lighter waters closer to the surface. How and where heat and salt mix across waters of different densities is important as this sets up the global ocean circulations and transport of heat from the tropics to the poles. This ocean mixing is influenced greatly by the winds and tides that churn up the ocean and generate internal waves. These waves that propagate in the interior of the ocean rather than just at the the surface, and are made possible by the ocean's stratification. These waves are very difficult to observe and so our understanding of their generation, propagation and breaking is an active field of research. Here, we demonstrate the existence of a new type of internal wave that is generated by storm systems blowing above submerged features on the seafloor. We found that under the right circumstances, these waves could be up to $\sim 50\%$ as strong as another type of internal wave which is known to be a large contributor to mixing. We argue that these novel internal waves are worthy of further study to better understand how they might fit into the ocean mixing picture.

## 1. Introduction

Internal waves (IWs), which manifest as vertical oscillations in astratified fluid, permeate the world's oceans. IWs are important to the fields of physical oceanography and climate science more broadly due to their significant contribution to ocean mixing and momentum transfer (Melet et al. 2013; Shakespeare and Hogg 2019). Global estimates of the energy contained by the internal wave field are supported by sparse in-situ observations and satellite altimetry (Whalen et al. 2018; Zhao et al. 2016). However, capturing the spatial variability of internal waves, and in turn their contribution to local episodic mixing, remains an ongoing challenge in oceanography, particularly in the deep ocean where observations are especially sparse. A further complication is that many types of internal wave can contribute both to the local mixing at the generation site, but also can carry their energy great distances to enhance mixing in remote locations (Waterhouse et al. 2014).

Ocean models can provide insights where observations are lacking, and accurately capturing internal wave induced mixing in numerical models is a large area of study. Some approaches to this problem such as Laurent and Garrett (2002) and Lavergne et al. (2020) construct spatially varying maps of the wave field by parameterising different wave generation mechanisms. This method has shown promise in matching observations where they are available (Lavergne et al. 2020), but an unavoidable source of error in such approaches comes from any processes that are omitted. By estimating the importance of this missing physics, we can increase our understanding of how well wave-induced mixing is represented in numerical models.

The bulk of internal waves begin their life-cycle at the boundary of the ocean – either at the surface generated via winds (Thomas and Zhai 2022), or near the bottom as a result of flow over topography (Musgrave et al. 2022). Inertial oscillations at the surface are readily excited by the wind, which in turn generate near-inertial waves that can propagate downwards, beyond the mixed layer (D'Asaro 1985). These waves are most prominent in areas of highly

*Corresponding author*: A. J. Barnes, ashley.barnes@anu.edu.au

variable winds and in the wake of individual storm systems, and can propagate thousands of kilometers horizontally away from their generation site (Alford 2003). These surface-generated waves also propagate vertically, typically reaching the seafloor weeks after their generation (Kunze and Sanford 1984; Ma et al. 2022) where they may scatter, dissipate or reflect depending on the local topography (Igeta et al. 2009).

Topography also plays a key role in the generation of internal waves. When non-wave flows interact with topography they lead to vertical motions, and thereby radiate internal waves due to the restoring effect of the stratification. Examples of such interactions principally include the barotropic tide (Bell 1975), as well as geostrophic currents (Nikurashin and Ferrari 2011). These two processes together contribute a similar amount of energy to the internal wave field as the surface-generated near-inertial waves (Wunsch 1998; Egbert and Ray 2000).

There is an indirect connection between wind-generated and topographically-generated internal waves. Wind forcing energises mean and transient geostrophic currents (Wunsch 1998), which in turn shed energy at the ocean bottom via topographic lee waves (Nikurashin and Ferrari 2010). Nikurashin and Ferrari (2011) estimated that 20% of energy input to geostrophic flows through synoptic scale wind forcing was converted to lee wave generation. However, this estimate does not consider how a transient bottom velocity, induced by storms or other shorter timescale weather patterns, might influence wave generation and mixing at the seafloor. A recent observational study by van Haren (2020) found evidence for enhanced mixing in the depths of the Mariana Trench coinciding with the passage of a cyclone overhead. A mooring detected patterns in the stratification similar to that of breaking internal waves within hours of the arrival of the storm. The rapid timescale and close proximity of the mixing to the storm suggest that dissipation of downwards propagating near-inertial waves are unlikely to account for observations, leaving the mechanism as an open question. Furthermore, Waterhouse et al. (2022) used global lowered acoustic doppler current profiler observations to identify geographic regions where upgoing rotary shear exceeded downgoing in the bottom 1000 m of the ocean. Rotary shear is usually dominated by near-inertial internal waves, and these results thus suggest the presence of additional sources of bottom generated near-inertial waves in these regions.

In this work, we investigate internal waves that are generated by a mechanism that can be thought of as a combination of the two main generation mechanisms: near-inertial waves from surface winds and internal tides from barotropic flow over topography. We demonstrate that wind-driven oscillations at the ocean's surface, close to the inertial frequency, can generate secondary, upwards-propagating internal waves at the bottom topography, in addition to the regular downward-propagating near-inertial waves. The proposed mechanism is as follows. When the wind-driven oscillations imprint on sea surface height, there is a rapid change in hydrostatic pressure at the ocean bottom, faster than the timescale at which internal isopycnal surfaces can adjust (Stewart et al. 2021). The result is the generation of an oscillatory bottom flow forced by the changes to hydrostatic pressure. In the presence of topography, this oscillatory flow may then generate internal waves in a similar fashion to the barotropic tide (Bell 1975). In the ocean, we expect these waves to be present in the wake of a storm. Given that storms convert large amounts of wind energy into inertial oscillations and in turn near-inertial waves (Sanford et al. 2011; Whalen et al. 2018), the coincidence of a storm directly above topographic features would provide the most pronounced generation. The hypothesised "topographic near-inertial waves" (as we refer to them hereafter) have, to our knowledge, not been studied before and thus it is unknown whether they constitute a significant contribution to the ocean internal wave field.

The next section outlines the model setup, as well as the method we used for separating the waves of interest from the rest of the flow. Then, the results section 3 includes a qualitative demonstration of these bottom near-inertial waves, followed by a quantitative analysis of the wave energy for various perturbation experiments. Finally, we conclude in section 4 by arguing that the results suggest wave generation significant enough to warrant further study using both observations and realistic ocean model configurations.

## 2. Methods

To study topographic near-inertial wave generation mechanism, we design an idealised numerical experiment as shown in Figure 1. The Modular Ocean Model version 6 (MOM6; Adcroft et al. (2019)) is run in an isopycnal configuration with 5 layers at 2 km horizontal resolution, 4000 m deep water and 4000 km by 4000 km horizontal extent. The eastern and western boundaries are re-entrant to allow zonal symmetry, and radiative open boundary conditions as described by Orlanski (1976) are utilised at the northern and southern boundaries to reduce spurious reflections. The model is initialised from rest with equally spaced isopycnal heights and with a linear stratification. For our control experiment, a Coriolis parameter $f = -10^{-4}$ s$^{-1}$ mimics the southern mid-latitudes, a constant buoyancy frequency of $N = 20f$, and a 500 m tall Gaussian ridge with half-width 12.5 km, meridionally symmetric ridge running north to south through the domain is placed in the centre.

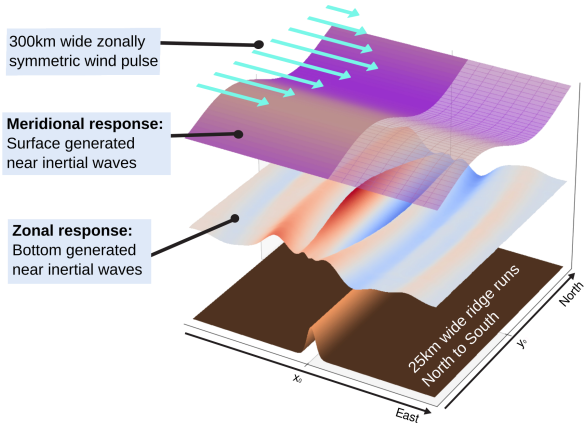


FIG. 1: A schematic of the model configuration, including the isopycnal displacements associated with both the surface and bottom generated near-inertial wave responses. Note that the vertical scales of the waves have been exaggerated, and that two layers are shown separately for illustrative purposes, having been filtered using the zonal symmetry of the surface near-inertial wave response. The zonal and meridional centre lines as referred to in the text are denoted by $x_0$ and $y_0$ respectively.

The model is forced only by a zonally symmetric 12-hour pulse of zonal wind stress given by

$$\tau(y,t) = \begin{cases} \tau_0 \sin^2\left(\frac{4\pi y}{L_\tau}\right) & 0 \le t \le \frac{T_\tau}{2}, \\ -\tau_0 \sin^2\left(\frac{4\pi y}{L_\tau}\right) & \frac{T_\tau}{2} < t \le T_\tau, \\ 0 & T_\tau < t, \end{cases} \tag{1}$$

where $\tau_0$ is the peak wind stress, $L_\tau$ the meridional extent of the wind stress, and $T_\tau$ the forcing duration. This pulse has a spatial pattern that is centred on the middle of the domain and is a squared sinusoid in the meridional direction with $L_\tau = 300$ km width. The magnitude, size, and duration of the pulse were designed to simulate the passing of a storm system overhead, and to minimise the induced mean flow in order to simplify analysis.

A challenge in studying topographic near-inertial waves is that, even in a highly idealised domain, the waves exist in the presence of other near-inertial oscillations. To simplify the separation of topographic waves from non-propagating inertial oscillations, surface generated near-inertial waves and their corresponding topographic scatter, the experiment was designed with a high degree of symmetry. The wind pulse is zonally symmetric, so that any surface generated near-inertial waves will propagate meridionally. This implies zonally propagating waves are a result of interactions with the topography, and so this zonal component would contain the waves of interest. (Note that since this experiment is conducted on an $f$-plane, wind generated near-inertial waves propagate both north and south, as opposed to on a $\beta$-plane where they would propagate equatorward only.)

Even with this simplification, these zonally propagating waves are still superimposed on the aforementioned background oscillations. However, along the centre line of the domain denoted by $x_0$ in Figure 1, there is a node in the isopycnal height displacements of the surface-generated near-inertial waves (as shown in Figure 1), eliminating the need to account for extraneous deviations to isopycnal heights.

In order to calculate the total energy of topographic near-inertial waves, longitude-depth transects of velocity, $u_i$, and isopycnal displacements, $\eta_i'$, are taken along this centre line, where the subscript $i$ denotes the $i$-th layer counting from the top. We take the Fourier transform in zonal wavenumber $k$ and frequency, $\omega$, and then filter out sub-inertial frequencies and zero wavenumber signals. This procedure ensures that the filtered $\hat{u}$ and $\hat{\eta}'$ contain neither components of the mean flow, nor that of non-wave barotropic, $x$-uniform inertial oscillations that exist in the absence of topography. Here, hats denote discrete Fourier transforms. By employing Parseval's theorem, the total wave energy along this 2D slice $E_B$ averaged in time can be expressed in phase space via,

$$E_B = \frac{\rho_0}{2\Delta T} \iint_{-\infty}^{\infty} \sum_{i=1}^{n} \left( g' |\widehat{\eta_i'}|^2 + H_i |\widehat{u_i}|^2 \right) \mathrm{d}\omega \, \mathrm{d}k, \tag{2}$$

where $\Delta T$ is the experiment run time, $H_i$ is the equilibrium layer thickness, $\rho_0$ the reference density, $g'$ the reduced gravity corresponding to our linear stratification profile, $n$ the total number of layers.

It is helpful to provide context for the wave energy of our idealised experiment by comparing it to metrics well understood in the real ocean, namely the wind work and energy conversion to surface generated near-inertial waves. The wind work directly over the Gaussian ridge (defined as two standard deviations either side of the ridge's centre) is used to compare the conversion rate of wind work to bottom near-inertial waves.

Due to the geometry of the experiment, the surface generated near-inertial wave energy cannot be directly compared to that of the bottom generated, as the waves exist in different areas of the domain and thus experience different amounts of wind forcing. To isolate the surface generated near-inertial waves, we use a latitude-depth slice far from the topography and perform analysis in the same manner to the topographic near-inertial waves. The total wave energy along this 2D slice $E_B$ is then calculated using a meridional version of equation (2) along with the corresponding wind work.

## 3. Results

### *a. Qualitative wave filtering*

In order to qualitatively check for the existence of topographic near-inertial waves, the zonal velocity and isopycnal displacements along the centre-line of the domain are calculated. Although the isopycnal displacements need no processing, the horizontal velocity field contains the wind generated inertial oscillations present throughout the domain. The zonal velocity was first processed by subtracting the zonal mean and taking a super-inertial high-pass filter to remove any mean flow imparted by the wind pulse. Figure 2 shows a zonal transect along the centre-line of the domain, with the processed horizontal velocity and exaggerated isopycnal displacements at four points in time separated by fractions of the 17 hour inertial period. During the period of wind forcing, beams of internal waves can be seen propagating away from the topography (Fig. 2a); as time proceeds the beams reflect from the surface (Fig. 2b) and propagates back into the domain (Fig. 2c,d). Changes to the phase at the time snapshots show that the frequency is slightly higher than inertial, consistent with topographic near-inertial waves.

By assessing the properties of the waves, we attain further evidence of internal wave generation. Figure 3a shows a Hovmöller diagram of the isopycnal displacement of the second layer below the surface along the centre-line of the domain. Eastward and westward propagating wave signals, including several superimposed vertical modes, can be seen fanning out from the topography. The corresponding power spectrum of the isopycnal displacement is depicted in Fig. 3b together with the vertical modes expected from the hydrostatic dispersion relation,

$$\omega^2 = f^2 + N^2 \frac{k^2}{m^2}, \tag{3}$$

where $k$ is the zonal and $m$ the vertical wavenumbers. Note that in (3) the meridional wavenumber $\ell$ is omitted from the numerator as we assume that $k^2 \gg \ell^2$ due to the width of the hill being $\sim 30$ times smaller than that of the meridional wind band. This approximation introduces a small amount of error and may explain the discrepancy between the overlaid vertical modes and the numerical data in Figure 3b. The qualitative similarity between the calculated vertical modes from the dispersion relation (3) and the peaks in the power spectrum provides conclusive evidence that the waves shown in Fig. 3a are internal waves.

Other well-understood internal wave-generation mechanisms can be ruled out as having caused the waves shown in Figure 3. Firstly, consider topographic lee waves excited by a mean flow. Although there is a westwards mean flow imparted by the wind pulse, it is too small to meet the $f < kU_0$ condition required to support topographic lee waves. This inference is further supported by the east-west symmetry in the wave field visible in Figure 3a, ruling out topographic lee waves from a mean flow. Secondly, bottom internal waves appear immediately after the wind pulse is initialised. This rapid response precludes the scatter of surface near-inertial waves as an explanation for the signal, as such a mechanism would result in a time lag of (at least) days for the surface-generated waves to reach the bottom (Ma et al. 2022). Given the lack of tides, instabilities and nonlinear dynamics in this experiment, other established mechanisms are not able to explain these upwards propagating waves either. We thus infer that the only plausible mechanism to generate the waves seen in figures 2 and 3 is the topographic near-inertial mechanism outlined in section 1.

### *b. Conversion of wind work to wave energy*

Having established the existence of topographic near-inertial waves in our configuration, we now proceed to calculate the conversion rate of wind work to wave energy as described in section 2. As shown in Table 1, the surface near-inertial waves account for 50% of the incident wind work compared to 3% for the topographically generated waves. Considering that the former are a major component of the internal wave field, a source of internal waves with $\sim 10\%$ the strength is a significant result.

Since the idealised experiment exaggerates the energy conversion for surface near-inertial waves compared to the 12-20% expected from Alford (2020), comparing generation of the two types of near-inertial waves is arguably a more useful metric than the total conversion rate. According to our results, the topographic near-inertial waves represent an energy pathway 10% as large as the surface near-inertial waves, which suggests that these waves could pose a significant source of additional wave generation in the deep ocean.

### *c. Perturbation experiments*

We run experiments by varying the wind pulse, topography shape and stratification to assess which factors the energy conversion rate, as well as the total wave energy are most sensitive to. It is clear that each of the variables tested alters energy of the topographic near-inertial waves by one or more order of magnitude (solid black lines, Figure 4). However, the behaviour of the conversion rate (solid blue lines) is markedly different to the total wave energy when varying some parameters. For instance, increasing the forcing strength elevates the energy of topographic near-inertial waves by 4 orders of magnitude (Figure 4a), but has no impact on the conversion rate. By considering both of these metrics, more can be determined about the underlying wave generation mechanism.

Firstly, the wind forcing was altered, modifying its strength, meridional width and duration (Fig. 4a-c). Considering the forcing strength perturbation shown in Fig. 4a,

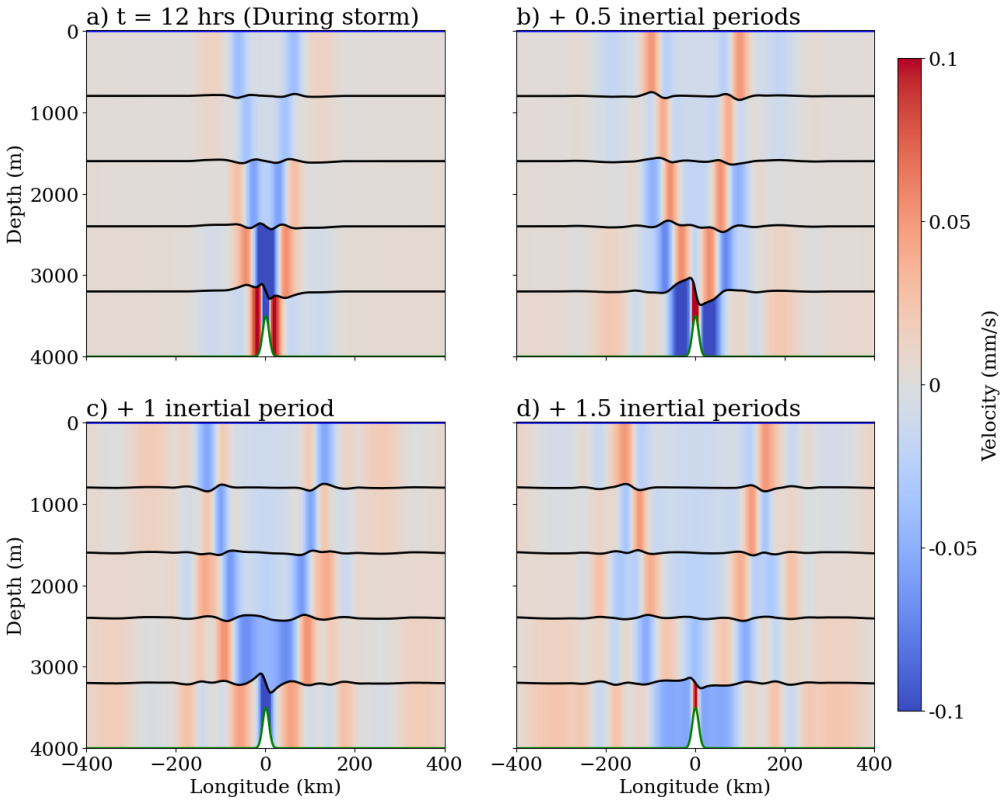


FIG. 2: Zonal transect showing zonal velocity and exaggerated isopycnal displacements from numerical simulation at four different time snapshots. Velocity values have had their zonal mean removed, and the isopycnal heights are exaggerated by a factor of 1000.

TABLE 1: Wind energy conversion rates for default experiment.

| | Wind work (kJ) | Wave energy (kJ) | Conversion rate |
|---|---|---|---|
| Topographic (zonal) NIWs | $10^5$ | $3\times10^4$ | 3% |
| Wind (meridional) NIWs | $10^5$ | $5\times10^6$ | 50% |

we observe an increase in both surface and topographic near-inertial wave generation (black lines), whilst the energy conversion rate remains steady (blue lines). Fitting the bottom near-inertial wave energy curve to a quadratic curve, we find a correlation coefficient of 0.99. Thus we conclude that the wave energy is proportional to the square of the wind stress purturbation.

When altering the duration of the wind forcing pulse (Fig. 4b), a maximum appears around 12 hours, corresponding to a frequency 40% faster than the Coriolis frequency. Aside from the 'strength' experiment, the wind stress pattern is modulated to ensure that the integrated wind stress amplitude remained constant. Generally, wind driven responses are greatest at the resonant inertial frequency, but internal wave generation is only supported at super-inertial frequencies. The wave energy flux increases with frequency, while the non-wave response decreases, meaning that we expect a peak in the bottom near-inertial wave generation at a frequency greater than $f$, consistent with our results.

In order to assess the importance of the spatial scale of the wind on the bottom velocity response, the meridional extent of the forcing profile was modified. In Fig. 4c, the surface near-inertial generation grows monotonically with width, while the topographic near-inertial generation peaks at ~200 km width. Aside from the ridge, the wind profile is the only source of spatial inhomogeneity in the domain. The wind stress is communicated to the interior through

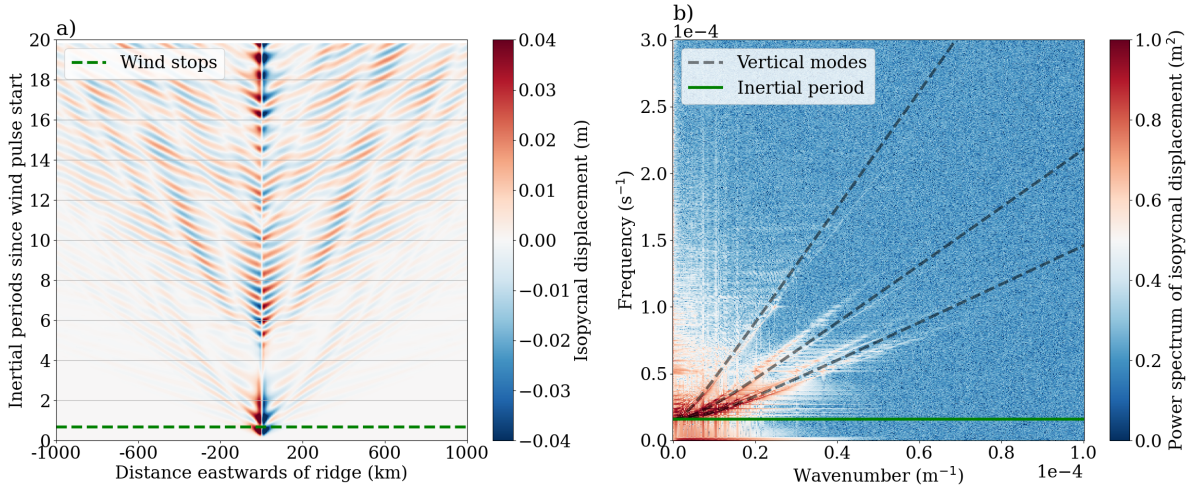


FIG. 3: a) Hovmöller diagram of the isopycnal displacement in the second layer at the centre line b) Corresponding power spectrum showing the theoretical locations of the vertical modes 1 to 3 (dashed black lines) and inertial frequency (green line).

spatial gradients that drive convergence and divergence of the surface layer flow, creating gradients in the hydrostatic pressure. Thus, in the extreme case of a spatially uniform wind profile, we expect that there would be no mechanism to generate the bottom flow necessary to support the topographic near-inertial waves. The modest reduction in wave energy with increasing forcing width is consistent with this expectation. However, this result implies is that storms must consist of a wind profile that appears homogenous for spatial scales larger than 1000 km before local homogeneity becomes important enough to suppress wave generation, which would not occur outside of an idealised setting. Our results thus suggest that wave generation is greatest for storms larger than 200 km.

The second series of tests conducted relate to the shape of the topography (Fig. 4d,e). As the ridge height increases, the energy conversion rate increases quadratically (with correlation coefficient 0.95) up to 24% for the 800 m ridge (solid blue line in Fig. 4d). As expected, the surface generation of near-inertial waves is independent of the ridge height.

The width of the ridge (Fig. 4e) also corresponds to increasing topographic wave generation, but to a lesser extent. Although the overall wave energy increases with increasing width, the conversion rate decreases due to the larger area over which the incident wind work is integrated as described in section 2. This means that while the total wave energy increases, the energy conversion per unit area decreases. This result is likely due to the less steep topographic slope being less efficient at generating waves.

Finally, alterations to stratification also have a significant impact on topographic wave generation. Wave energy vanishes as expected for low levels of stratification where internal waves are no longer supported, and increases linearly (correlation coefficient 0.97) up to doubled stratification in Figure 4f. Caution should be taken in interpreting the results for weak stratification ($N \sim f$), since the hydrostatic assumption used by the numerical model is no longer a valid description for internal waves.

Due to the similarities between the generation of topographic near-inertial waves and other internal waves generated by an oscillating background flow, existing theory for other topographically generated waves can be applied in interpreting our results. The conversion rate $C$ of energy from an oscillatory flow of amplitude $U_0$ to buoyancy frequency $N$, topography height $h$, and horizontal wavenumber $k$, are related by (Legg 2021):

$$C = \frac{1}{4}\rho_0 U_0^2 h^2 N k, \tag{4}$$

where $\rho_0$ is the reference density. Although topographically generated near-inertial waves differ from the lee waves of Legg (2021) in that the oscillatory flow is excited by winds, Eq. (4) holds for our study to leading order if $U_0$ refers instead to the characteristic amplitude of the wind-induced velocity.

While we have not varied $U_0$ directly, in a linear regime the magnitude of the velocity response is proportional to the surface stress, so in turn $|\boldsymbol{u}|^2 \sim |\boldsymbol{\tau}|^2$, consistent with the quadratic relationship between $\tau_0$ and both topographic and surface wave energy in Figure 4a. Similarly, we find that the topographic near-inertial wave energy scales quadratically with ridge height, as does buoyancy frequency linearly. In Eq. (4), the horizontal wavenumber is set by that of the sinusoidal topography used in their study. Equa-

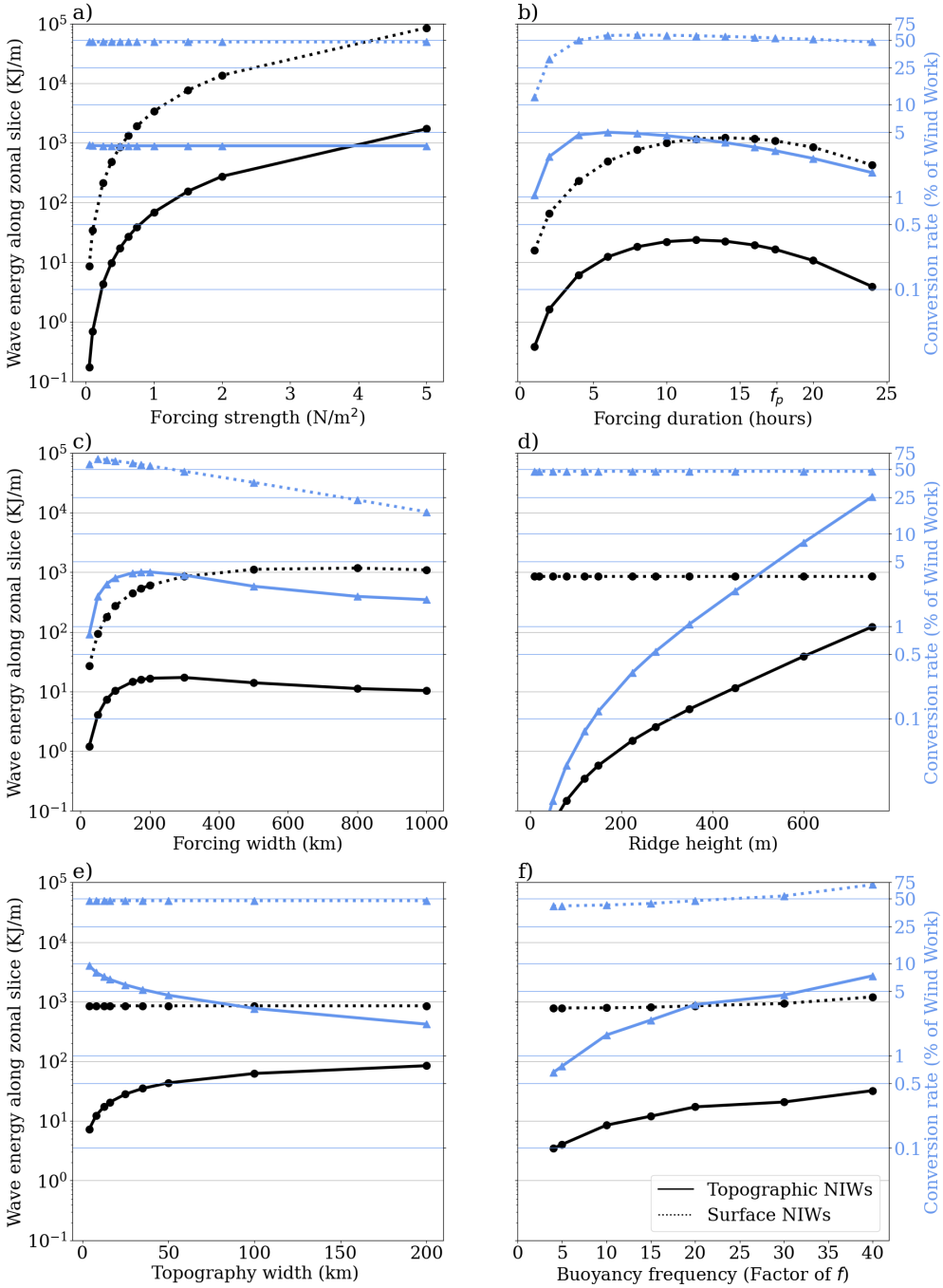


FIG. 4: Perturbation experiments in which the following are varied: a) Peak forcing strength; b) Duration of the wind forcing pulse shown in equation (1) with the Coriolis period $f_p$ labelled on the abscissa; c) Latitudinal extent of the Gaussian wind profile measured to two standard deviations; d) Height of the Gaussian ridge; e) Zonal extent of the ridge and f) Stratification, shown as the buoyancy frequency, $N$, divided by Coriolis, $f$.

tion (4) can also be applied to topography width, hereby $L_t$. If we instead consider the dominant wavenumber of the ridge to be set by its width $L_t$, then $k \sim 1/L_t$. This is consistent with the our results in Figure 4 in which we find a negative —although not $1/L_t$— trend in wind work to topographic near-inertial wave energy conversion with

increasing ridge width, in contrast to the increasing total wave energy. Intuitively, this means that for wider, and in turn less steep topography, the wind work to wave energy conversion per unit area decreases.

## 4. Discussion and conclusions

We demonstrate, for the first time, the existence of a new class of topographic near-inertial internal waves that are generated by high-frequency winds rapidly creating near-bottom flows which interact with topography to radiate waves. This generation mechanism is showcased using an isopycnal model forced by a wind pulse that mimics a storm. The idealised model setup is carefully constructed to enable a clean separation of our proposed waves from the more common surface generated near-inertial waves and to eliminate any significant mean flow that could generate lee waves and largely eliminate any mean flow that could radiate lee waves

We find that the topographic near-inertial waves are associated with a non-negligible pathway for the conversion of wind work to wave energy. In the control experiment with a 500 m ridge, we find a conversion rate of 3% for bottom generated near-inertial waves and that rises up to 24% for a ridge with height of 750 m. Compared with the 50% for surface generated near-inertial waves in both of these experiments, our results suggest that the topographic near-inertial waves could contribute significantly to the local internal wave field when a storm passes overhead. Being generated at the seafloor, these topographic waves may be especially important as they come at near-inertial frequencies and hence, exhibit high vertical shear, meaning that they are likely to dissipate close to the ocean bottom and contribute significantly to abyssal mixing.

Based on our perturbation experiments, the surface forcing properties that would produce the strongest conversion rate of wind work to topographic near-inertial wave energy are wind stresses stronger than 2 N m$^{-2}$ with timescales $\sim$ 40% faster than the Coriolis frequency and with spatial scales greater than 200 km. Likewise, within the range of the tested parameters, prominent topographic features support more energetic waves. The dependence of wave generation on topography, stratification, and forcing is broadly consistent with the previous scalings for topographic lee waves by Legg (2021) (Eq. (4)) lending further evidence to the proposed mechanism of generation.

Here, we studied the generation of topographic near-inertial waves in a highly idealised domain to cleanly separated them from other flow features. An important next step is to identify the waves in more realistic simulations. However, delineating topographic near-inertial waves from other flow factors due to challenges posed by the generation mechanism.

As the topographic near-inertial waves are produced as a secondary response from wind forcing, much care is needed to extract them effectively from other dynamical features in the domain. Our experiments were carefully designed to separate the topographic near-inertial waves from other flow features as cleanly as possible. Consequently, this limited the scope of our study to simple dynamics, topographic features, and surface forcing profiles. To investigate topographic near-inertial waves in a more realistic numerical simulation or with observations, these intricacies of disentangling them from other flow features will need to be handled carefully. One option could be to exploit the difference in vertical propagation between the topographic and wind-generated near-inertial waves. If a filter were used to separate the upwards and downwards propagating signals, perhaps following the spectral approach employed by Olbers and Eden (2017) or Waterhouse et al. (2022), one could identify areas of increased vertical energy flux beneath storm systems. By looking only at a limited horizontal radius from the storm, downwards propagating near-inertial waves would not have had enough space to reach the seafloor and reflect or scatter. However, one would still need to remove the background internal wave fields, among other oscillatory signals that could obscure the waves of interest. To obtain a stronger signal, a statistical approach could be employed, e.g., averaging over many storm events in several locations above regions of varying topographic prominence. At each location, measurements of the bottom mixing could be taken both in the absence and presence of an overhead storm. Future studies could employ this approach on high resolution model outputs or observations.

As hypothesised above, the topographic near-inertial waves may be an important contributor to deep ocean mixing, but the exact extent and location of mixing induced remains an open question. Our study was designed to maximise wave generation, and hence mechanisms for wave breaking and dissipation were intentionally either removed or suppressed. It remains possible that in more realistic conditions the waves would immediately break, become trapped, or otherwise dissipate close to the generation site. Further study is therefore needed to understand how these waves appear in the real ocean. If the class of waves proposed here are responsible for the intensified near-bottom mixing observed by Vic et al. (2019) or van Haren (2020), then one could assess their impact indirectly by measuring the bottom mixing rates at other intersection points of topographic features and storm systems. This could be done either with existing moorings, or by analysing model outputs of high resolution ocean models with more realistic forcing and bathymetry. The advantage of using a high-resolution ocean model is that the effects of tides could easily be removed, so enhanced internal wave generation or breaking at the bottom in the presence of storms could more easily be teased out.

In conclusion, we have studied a novel internal-wave generation mechanism whereby fast oscillations in surface

wind directly above a topographic feature result in bottom generated near-inertial waves. The rate of energy conversion from wind work to wave energy reaches 50% of the well-established surface near-inertial waves. By separating the topographic near-inertial waves from other dynamical features in our idealised experiments as cleanly as possible, we found that wave energy scales in a way consistent with existing internal wave theory. Further study of topographic near-inertial waves in ocean observations and realistic models would help us clarify how these waves might fit into the broader internal wave spectrum, and our picture of abyssal mixing.

*Acknowledgments.* Computational resources were provided by the National Computational Infrastructure at the Australian National University, which is supported by the Commonwealth Government of Australia. A.J.B. acknowledges his PhD stipend provided by the Australian Research Training Program, as well as the funding from the Australian Research Council's Centre of Excellence for Climate Extremes. N.C.C. acknowledges funding from the Australian Research Council under DECRA Fellowship DE210100749. A.J.B. would like to thank Jemma Jeffree for their proofreading and support, as well as Andrew Kiss and Ellie Ong for their mentorship and suggestions during the study.

*Data availability statement.* Scripts used to generate figures and perform analysis will be made publicly available at `github.com/ashjbarnes/topographic-NIWs` on the acceptance of this manuscript. The MOM6 source code can be found at `github.com/mom-ocean/MOM6`. Data from the model runs, as well as post-processed data for reproducing figures will be made available in a Zenodo repository upon acceptance of the manuscript.

## References

Adcroft, A., and Coauthors, 2019: The GFDL Global Ocean and Sea Ice Model OM4.0: Model Description and Simulation Features. *Journal of Advances in Modeling Earth Systems*, **11 (10)**, 3167–3211, https://doi.org/10.1029/2019MS001726.

Alford, M. H., 2003: Redistribution of energy available for ocean mixing by long-range propagation of internal waves. *Nature*, **423 (6936)**, 159–162, https://doi.org/10.1038/nature01628.

Alford, M. H., 2020: Revisiting Near-Inertial Wind Work: Slab Models, Relative Stress, and Mixed Layer Deepening. *Journal of Physical Oceanography*, **50 (11)**, 3141–3156, https://doi.org/10.1175/JPO-D-20-0105.1.

Bell, T. H., 1975: Topographically generated internal waves in the open ocean. *Journal of Geophysical Research (1896-1977)*, **80 (3)**, 320–327, https://doi.org/10.1029/JC080i003p00320.

D'Asaro, E. A., 1985: The Energy Flux from the Wind to Near-Inertial Motions in the Surface Mixed Layer. *Journal of Physical Oceanography*, **15 (8)**, 1043–1059, https://doi.org/10.1175/1520-0485(1985)015⟨1043:TEFFTW⟩2.0.CO;2.

Egbert, G. D., and R. D. Ray, 2000: Significant dissipation of tidal energy in the deep ocean inferred from satellite altimeter data. *Nature*, **405 (6788)**, 775–778, https://doi.org/10.1038/35015531.

Igeta, Y., Y. Kumaki, Y. Kitade, T. Senjyu, H. Yamada, T. Watanabe, O. Katoh, and M. Matsuyama, 2009: Scattering of near-inertial internal waves along the Japanese coast of the Japan Sea. *Journal of Geophysical Research: Oceans*, **114 (C10)**, https://doi.org/10.1029/2009JC005305.

Kunze, E., and T. B. Sanford, 1984: Observations of Near-Inertial Waves in a Front. *Journal of Physical Oceanography*, **14 (3)**, 566–581, https://doi.org/10.1175/1520-0485(1984)014⟨0566:OONIWI⟩2.0.CO;2.

Laurent, L. S., and C. Garrett, 2002: The Role of Internal Tides in Mixing the Deep Ocean. *JOURNAL OF PHYSICAL OCEANOGRAPHY*, **32**, 18.

Lavergne, C., and Coauthors, 2020: A Parameterization of Local and Remote Tidal Mixing. *Journal of Advances in Modeling Earth Systems*, **12 (5)**, https://doi.org/10.1029/2020MS002065.

Legg, S., 2021: Mixing by Oceanic Lee Waves. *Annual Review of Fluid Mechanics*, **53 (1)**, 173–201, https://doi.org/10.1146/annurev-fluid-051220-043904.

Ma, Y., D. Wang, Y. Shu, J. Chen, Y. He, and Q. Xie, 2022: Bottom-Reached Near-Inertial Waves Induced by the Tropical Cyclones, Conson and Mindulle, in the South China Sea. *Journal of Geophysical Research: Oceans*, **127 (6)**, e2021JC018 162, https://doi.org/10.1029/2021JC018162.

Melet, A., R. Hallberg, S. Legg, and K. Polzin, 2013: Sensitivity of the Ocean State to the Vertical Distribution of Internal-Tide-Driven Mixing. *Journal of Physical Oceanography*, **43 (3)**, 602–615, https://doi.org/10.1175/JPO-D-12-055.1.

Musgrave, R., F. Pollmann, S. Kelly, and M. Nikurashin, 2022: Chapter 6 - The lifecycle of topographically-generated internal waves. *Ocean Mixing*, M. Meredith, and A. Naveira Garabato, Eds., Elsevier, 117–144, https://doi.org/10.1016/B978-0-12-821512-8.00013-X, URL https://www.sciencedirect.com/science/article/pii/B978012821512800013X.

Nikurashin, M., and R. Ferrari, 2010: Radiation and Dissipation of Internal Waves Generated by Geostrophic Motions Impinging on Small-Scale Topography: Theory. *Journal of Physical Oceanography*, **40 (5)**, 1055–1074, https://doi.org/10.1175/2009JPO4199.1.

Nikurashin, M., and R. Ferrari, 2011: Global energy conversion rate from geostrophic flows into internal lee waves in the deep ocean. *Geophysical Research Letters*, **38 (8)**, https://doi.org/10.1029/2011GL046576.

Olbers, D., and C. Eden, 2017: A Closure for Internal Wave–Mean Flow Interaction. Part I: Energy Conversion. *Journal of Physical Oceanography*, **47 (6)**, 1389–1401, https://doi.org/10.1175/JPO-D-16-0054.1.

Orlanski, I., 1976: A simple boundary condition for unbounded hyperbolic flows. *Journal of Computational Physics*, **21 (3)**, 251–269, https://doi.org/10.1016/0021-9991(76)90023-1.

Sanford, T. B., J. F. Price, and J. B. Girton, 2011: Upper-Ocean Response to Hurricane Frances (2004) Observed by Profiling EM-APEX Floats. *Journal of Physical Oceanography*, **41 (6)**, 1041–1056, https://doi.org/10.1175/2010JPO4313.1.

Shakespeare, C. J., and A. M. C. Hogg, 2019: On the Momentum Flux of Internal Tides. *Journal of Physical Oceanography*, **49 (4)**, 993–1013, https://doi.org/10.1175/JPO-D-18-0165.1.

Stewart, A. L., X. Chi, A. Solodoch, and A. M. Hogg, 2021: High-Frequency Fluctuations in Antarctic Bottom Water Transport Driven by Southern Ocean Winds. *Geophysical Research Letters*, **48 (17)**, e2021GL094 569, https://doi.org/10.1029/2021GL094569.

Thomas, L. N., and X. Zhai, 2022: Chapter 5 - The lifecycle of surface-generated near-inertial waves. *Ocean Mixing*, M. Meredith, and A. Naveira Garabato, Eds., Elsevier, 95–115, https://doi.org/10.1016/B978-0-12-821512-8.00012-8, URL https://www.sciencedirect.com/science/article/pii/B9780128215128000128.

van Haren, H., 2020: Challenger Deep internal wave turbulence events. *Deep Sea Research Part I: Oceanographic Research Papers*, **165**, 103 400, https://doi.org/10.1016/j.dsr.2020.103400.

Vic, C., and Coauthors, 2019: Deep-ocean mixing driven by small-scale internal tides. *Nature Communications*, **10 (1)**, 2099, https://doi.org/10.1038/s41467-019-10149-5.

Waterhouse, A. F., and Coauthors, 2014: Global Patterns of Diapycnal Mixing from Measurements of the Turbulent Dissipation Rate. *Journal of Physical Oceanography*, **44 (7)**, 1854–1872, https://doi.org/10.1175/JPO-D-13-0104.1.

Waterhouse, A. F., and Coauthors, 2022: Global Observations of Rotary-with-Depth Shear Spectra. *Journal of Physical Oceanography*, **52 (12)**, 3241–3258, https://doi.org/10.1175/JPO-D-22-0015.1.

Whalen, C. B., J. A. MacKinnon, and L. D. Talley, 2018: Large-scale impacts of the mesoscale environment on mixing from wind-driven internal waves. *Nature Geoscience*, **11 (11)**, 842–847, https://doi.org/10.1038/s41561-018-0213-6.

Wunsch, C., 1998: The Work Done by the Wind on the Oceanic General Circulation. *Journal of Physical Oceanography*, **28 (11)**, 2332–2340, https://doi.org/10.1175/1520-0485(1998)028⟨2332:TWDBTW⟩2.0.CO;2.

Zhao, Z., M. H. Alford, J. B. Girton, L. Rainville, and H. L. Simmons, 2016: Global Observations of Open-Ocean Mode-1 M2 Internal Tides. *Journal of Physical Oceanography*, **46 (6)**, 1657–1684, https://doi.org/10.1175/JPO-D-15-0105.1.